ACOUSTIC EMISSION DURING INTERGRANULAR STRESS CORROSION CRACKING

Dr. Mark A. Friesel and Dr. Russell H. Jones

Pacific Northwest Laboratory
Operated by Battelle Memorial Institute
Battelle Boulevard
Richland, WA 99352

INTRODUCTION

The physical and chemical processes taking place during intergranular stress corrosion cracking (IGSCC), in particular the effects of impurities on cracking mechanisms, have been the subjects of a research program sponsored by the Division of Materials Science, Office of Basic Energy Science, U. S. Department of Energy at Pacific Northwest Laboratory (PNL), operated by Battelle Memorial Institute. Acoustic emission (AE) was brought into the program because of the unique ability of AE methods to detect dynamic microscopic fracture processes. In this paper, the results of these tests are presented.

A number of processes occurring during IGSCC, transgranular stress corrosion cracking (TGSCC) and hydrogen embrittlement of steels and other metals have been identified as potential AE sources by various authors referenced below. It is not a simple matter to compare these results because of differences in materials, testing procedures, and the parameters examined. Where reported, AE behavior which was either consistent or not contradicted by others included the presence of burst-type AE associated with stress corrosion cracking (probably in contrast to "continuous" emission associated with e.g. dislocations), a tendency of AE signal amplitudes to increase with increasing grain size in a given material, an increased number of detected events from larger-grained material [1,2], and linear or exponential relationships between ringdown counts or AE event rates and crack growth rate [3,5], cumulative ringdown counts and crack length [2,3], and AE energy or cumulative AE events and crack area [1,2,4]. In another case, AE energy rate and crack growth rate were described as "clearly related [1]."

Equipment, Materials, and Procedure

The experimental equipment, setup, and test procedure is described elsewhere [6] and will be reviewed here only in brief. Test equipment is illustrated schematically in Fig. 1. Compact tension specimens of the materials (Table I) were notched and fatigue precracked. Dimensions were 6 x 7 x 0.9 cm for steel specimens, providing sufficient area for the AE sensors to be edge-mounted, while other specimens were 0.2 cm wide, and the sensor mounted by tapping a shallow hole in the specimen side. The

Review of Progress in Quantitative Nondestructive Evaluation, Vol. 9
Edited by D.O. Thompson and D.E. Chimenti
Plenum Press, New York, 1990

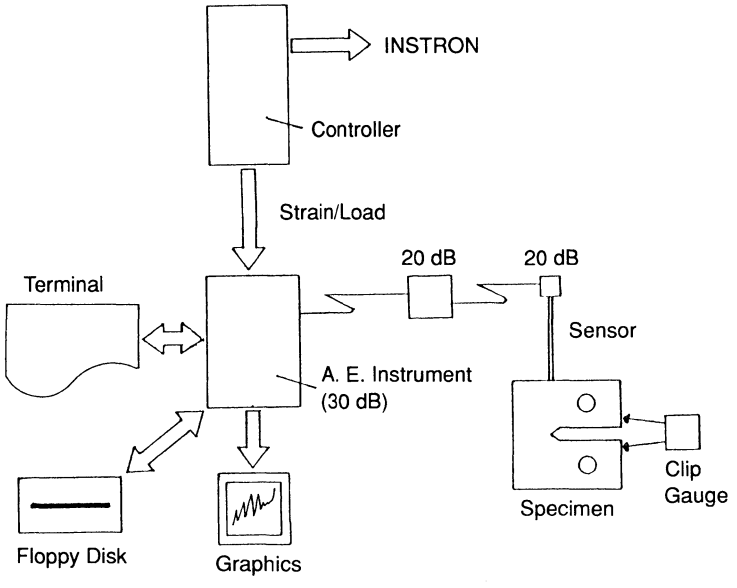

Fig. 1. Test Equipment Schematic

notch was 4.5 cm long cut parallel to the long axis. A short waveguide sensor was attached to the specimen and the specimen mounted to an Instron testing machine. The sample and machine grips were then coated with epoxy except along the expected crack line, and immersed in solution at the appropriate temperature and potential (Table II). The sensor was made of a PZT-5 crystal epoxied to a 24 cm long by 0.3 mm diameter 308-L stainless steel rod. The AE instrument was a Dunegan/Endevco 1032 for all but two of the tests, with threshold set to about 50 μV at the sensor output. A PNL instrument designed and built for the Naval Air Development Center [7] was used for the remaining tests.

Two or more of each specimen type except IMP were tested to insure repeatability of the test results. The consistently low number of events obtained from some specimens as described below helped assure that the specimen mounting assembly was not a source of noise. Results presented here are from three iron alloys labelled I01-2, IP1-4, and IMP-3; nickel alloys NP-9 and NA-4, and type 304 stainless steel SC6-4, SC6-6, and SC7-3.

The loading procedure was to increment the load quickly and hold for an extended period to allow crack growth rate measurements to be obtained. Generally, the tests were continued until the cracked specimen could no longer resist the applied load, at which point the test was terminated.

Results and Analysis

Results were obtained in terms of relationships between crack growth rate and crack length determined from COD gauge output (without compliance considerations), the number of AE events, event rate, signal amplitude and time. Ringdown counts and signal duration were also measured, but it was found that an exponentially decaying envelope imposed on the AE signals by the D/E 1032 usually caused impressive but erroneous measurements of these two parameters. On the PNL instrument, ringdown counts were not measured, and signal durations appeared to be independent of signal amplitude.

Table I. Material Compositions (appm.)

Material	Sample	S	P	Mn	C	N	O	Cr	Ni	Si
Fe	I01	30	36	100	30	20	1600	100	100	<200
Fe + 0.1P	IP1	33	1000	---	55	22	870	<100	<100	<200
Fe + 0.1P + 0.1Mn	IMP	34	1000	800	5	24	830	<100	<100	<200
Ni	NA	5	40	10	45	5	180	---	---	---
Ni + P	NP	5	300	---	20	---	0	---	---	---
304 Stainless*	CS6	.013	.013	1.72	.062	.065	---	18.48	8.75	0.39
304 Stainless*	CS7	.017	.046	1.74	.072	.036	---	18.53	9.33	0.46

*Values given in wt.%

Table II. Test Conditions

Sample	Heat Treatment Time (hrs)/Temp (°C)	Solution	Potential (mV)	Solution Temperature (°C)
I01	0.5/800 + 240/600	1N H_2SO_4	-600	RT
IP1	0.1/800 + 500/500	55% $Ca(NO_3)_2$	+750	60
IMP	4.0/850 + 500/500	55% $(Ca(NO_3)_2$	+750	60
NA	1.0/850 + 240/600	1N H_2SO_4	-300	RT
NP	1.0/850 + 240/600	1N H_2SO_4	+900	RT
CS6	Medium Sensitization	13 ppm $Na_2(S_2O_3)$	0	90
CS7	Sensitized	13 ppm $Na_2(S_2O_3)$	0	90

Table III. Test Results Summary

Specimen	Category	Estimated % Intergranular
IO1-2	I	>95
IP1-4	I/II	>95
IMP-3	II	>95
NA-4	III	50-80
NP-0	I	>95
SC6-4/6	I	60-80
SC7-3	III	>95

The test results could be divided into three main categories. Category I consists of those specimens which produced sufficient detectable AE to allow relationships between emission and mechanical parameters to be found, and for which these relationships are consistent. Category II contains specimens which show substantial emission, but with sporadic or inconsistent behavior, while Category III contains specimens which show little AE detectable at the present sensitivity level. Table III contains a summary of the test results.

In Category I are specimens IO1-2, IP1-4, NP-9, and the two SC6 specimens, with typical test data shown in Fig. 2. SEM micrographs of the fracture surfaces of four of the specimens are shown in Fig. 3 (SC6-4 is absent because the SEM was not available when the test was performed).

Specimens NP-9, SC6-4, and IP1-4 show behavior expected from past work by others cited above. As Fig. 4 illustrates, any changes in AE behavior with increasing crack growth rate should appear as a decrease in the event density, and an increase in event amplitudes. Specimen IP1-4 crack growth behavior differed somewhat from the other materials in that COD increased in a few discrete increments accompanied by high emission rates [6] rather than quasi-continuously, as per Fig. 2. Behavior of the

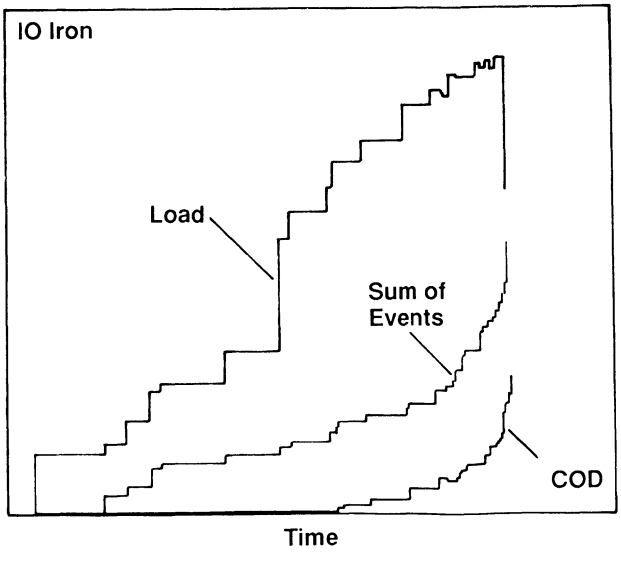

Fig. 2. Plot of Typical Raw Test Data.

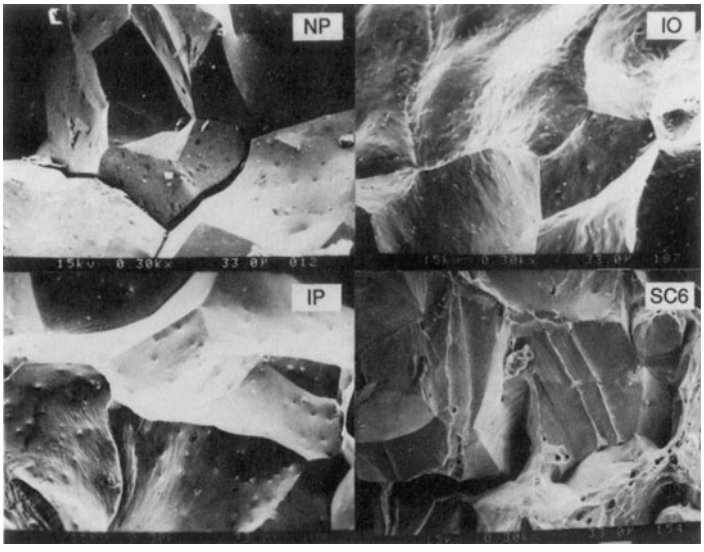

Fig. 3. Micrographs of Fracture Surfaces.

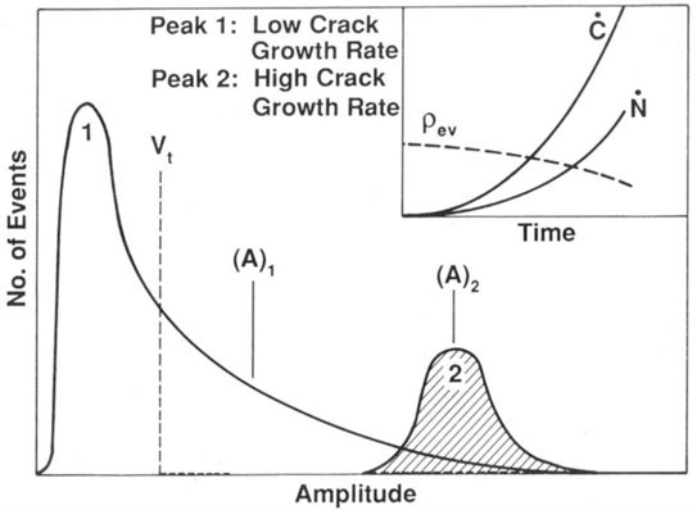

Fig. 4. Category I AE Behavior. $(A)_i$ = Mean Amplitude, V_t = Threshold Voltage, ρ_{ev} = Event Density, $\dot{C}$ and $\dot{N}$ are crack growth and AE event rates.

places this portion of IP1-4 iron in Category II and is described below, while later portions of the test showed behavior consistent with Category I. Changes in AE behavior in this specimen occurred as abrupt transitions between extended regions of constant AE event density, event rate, etc., a characteristic of other materials as well, which apparently has not been noted by other authors. Figure 5 shows AE behavior in two successive regions denoted IP-C and IP-D [8].

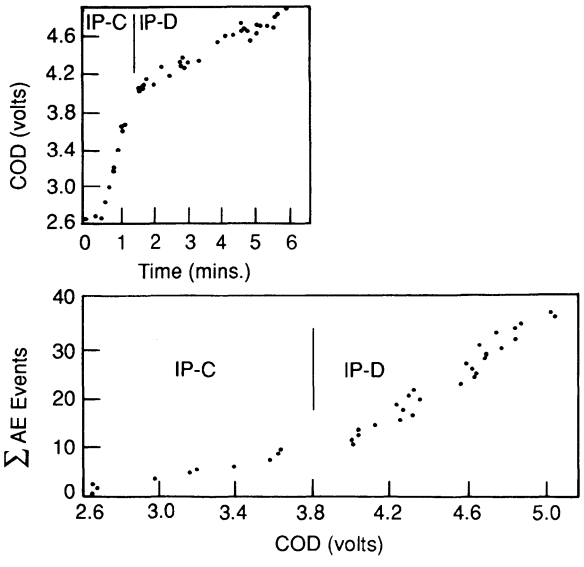

Fig. 5. AE Behavior in IP iron.

In IO1-2 iron, mean AE signal amplitude was found to decrease and event density increase at higher crack growth rate. These observations conflict with other Category I specimens, but the difficulty can be simply resolved. If the amplitude distribution peak occurs below the detection threshold at low crack growth rate, increased signal amplitudes caused by a higher crack growth rate allow a greater number of events to exceed the threshold for a given amount of crack growth. Since the signal amplitude is determined only for detected events, the mean of measured AE amplitudes can decrease if a large number of newly-detectable events have amplitudes close the threshold value.

Results from specimen IMP-3, and the early portion of IP1-4 belong to Category II. Figure 6 summarizes the IMP-3 data and indicates suspected sources. Acoustic emission signal amplitudes are highest in the early event cluster, tentatively associated with transition from the transgranular fatigue precrack to IGSCC. Emission in the second region occurred near where the highly slanted fracture surface began to grow back toward a flat configuration. Intergranular separations normal to the main fracture surface are the suspected sources of the detected emissions over this region. In IP1-4 iron, crack growth began during constant load in a region labelled IP-A as reported previously [6]. In this region, initiation of crack growth was accompanied by a cluster of high amplitude AE events from an unidentified source, which preceded detectable change in COD output.

Category III contains specimens NA-4 and SC7-3. These specimens produced little detectable emission during nearly pure IGSCC, probably because of low signal amplitudes and relative insensitivity of the detector.

Discussion

It seems significant that AE behavior appears essentially the same for many of the materials examined in these tests, and that qualitatively similar results were obtained from different materials and test conditions

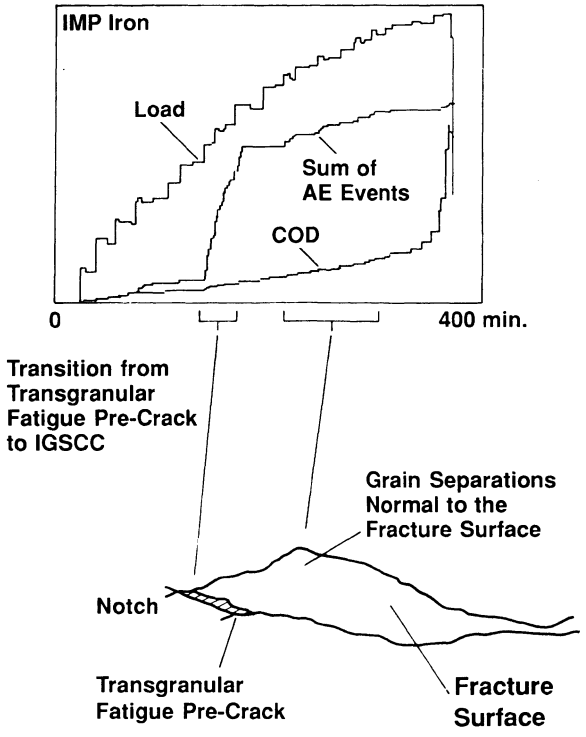

Fig. 6. IMP-3 Data.

by other researchers. From current data for example, as long as the crack growth rate remains constant or within a specific range, the AE event density is also constant. When this occurs, accumulated AE events are proportional to the total crack area, and the average AE event rate is likewise proportional to the crack growth rate in agreement with earlier observations. The AE energy and ringdown counts of a signal, for a given detection system, depends on the signal frequency, signal amplitude, and signal shape. Assuming a single active AE source mechanism and a sufficient number of events, the average values of these parameters will remain constant over successive regions of crack growth if the event density does not change, again producing previously observed results.

In general, materials with inclusions on the fracture surfaces visible at about 300x magnification were in Category I, while those without visible inclusions were in Category III. The authors speculate that grain boundary inclusions may lock adjacent grains together, pinning the crack faces and producing AE when the pins are abruptly broken. Supporting this interpretation, in IO1-2 iron the AE event density reached a value comparable to the density of visible fracture surface precipitates.

Other observations indicate that this general conclusion may require some modification. The NP-9 specimen was very noisy during nearly pure IGSCC, but the grain boundary inclusions were smaller than other Category I materials and closer to the size of the IMP-3 inclusions. In NP-9 therefore, precipitates may not play a role in AE production during IGSCC. In SC6-6 few precipitates were observed on the intergranular crack surfaces,

but were common in the ductile regions. If AE in this material is inclusion related, the AE source may be e.g. the rupture of ductile ligaments rather than IGSCC. Whatever the process, it causes the same general AE behavior as other materials which fail by nearly pure IGSCC. Although similar AE behavior was observed among all specimens in Category I, it seems evident that identification of the specific AE source mechanisms requires some additional research.

Finally, it is noted that substantial AE is produced in SC7 material, despite the above results. In subsequent experiments performed for the Electric Power Research Institute (EPRI) of Palo Alto where greater detection sensitivity was attained, the authors observed an estimated 1 AE event per 20 grains of crack growth.

REFERENCES

1. McIntyre, P. and G. Green, "Acoustic Emission During Stress Corrosion Cracking in High Strength Steels," British Journal of NDT, May 1978, pp. 135-140.
2. Padmanabhan, R., N. Suriyayothin, W. E. Wood, "Grain Size - Acoustic Emission Relationships in Hydrogen-Induced Delayed Cracking," Met. Trans. A, 14A, November 1983, p. 2357-2362.
3. Pollock, W. J., D. Hardie, and N. J. H. Holroyd, "Monitoring Sub-critical Crack Growth Due to Stress Corrosion or Hydrogen Embrittlement by Acoustic Emission," Br. Corr. Journal, 17(3), 1982, pp. 103-111.
4. A. Nozue and T. Kishi, "An Acoustic Emission Study of the Intergranular Cracking of AISI 4340 Steel," Journal of Acoustic Emission, 1(1), January 1982, pp. 1-6.
5. Yuyama, S., et al, "AE Analysis During Corrosion, Stress Corrosion Cracking, and Corrosion Fatigue Process on Type 304 Stainless Steel," Proceedings of Fifth International Acoustic Emission Symposium, Tokyo, 1980, pp. 115-124.
6. M. A. Friesel and R. H. Jones, "Acoustic Emission During Intergranular Stress Corrosion Cracking of Iron," Journal of Acoustic Emission, 7(2), April-June 1988, pp. 119-127. Note: Figure 13 in this reference has labels of regions IP-C and IP-D reversed. In Figure 5, 7.2 should read 0.2.
7. P. H. Hutton, et al, "Develop In-Flight Acoustic Emission Monitoring of Aircraft to Detect Fatigue Crack Growth - Final Report," Volume 2, NADC-81087-60, 1983.